Frequency and Voltage Stability Analysis of Grid-Forming Virtual Synchronous Generator Attached to Weak Grid

Li, Chang; Yang, Yaqian; Cao, Yijia; Wang, Lei; Blaabjerg, Frede

Published in:
IEEE Journal of Emerging and Selected Topics in Power Electronics

DOI (link to publication from Publisher):
10.1109/JESTPE.2020.3041698

Publication date:
2022

Document Version
Accepted author manuscript, peer reviewed version

This article has been accepted for publication in a future issue of this journal, but has not been fully edited. Content may change prior to final publication. Citation information: DOI 10.1109/JESTPE.2020.3041698, IEEE Journal of Emerging and Selected Topics in Power Electronics

Frequency and Voltage Stability Analysis of Grid-forming Virtual Synchronous Generator Attached to Weak Grid

Chang Li, Yaqian Yang, Yijia Cao, Senior Member IEEE, Lei Wang, Member, IEEE, Tomislav Dragicevic, Senior Member, IEEE, Frede Blaabjerg, Fellow, IEEE

***Abstract*—Virtual synchronous generator (VSG) control technique is widely used for the grid-friendly integration of renewable energy. However, when VSG is attached to a weak grid, it is prone to voltage and frequency instability, which aggravates the voltage quality and frequency quality at the point of common coupling (PCC), and in turn, pollutes the supplying quality for the loads. On the one hand, focusing on voltage stability, this paper proposes the impedance modeling for VSG in the synchronously inertial reference coordinates (SIRC) to measure the voltage stability of grid-tied VSG and identify the interaction between VSG and the weak power grid. Studies show that weak grid strength can lead to a wide-band oscillation of VSG. On the other hand, focusing on frequency instability, the motion equation has been put forward to illustrate the oscillation and dynamic deviation of frequency. The relationship between synchronizing ability of VSG and grid stiffness is discussed. Besides, this paper proposes an inertia-damping-strengthened control method to improve frequency stability. Finally, the theoretical analysis is compared with simulations and experiments.**

***Index Terms*—frequency stability, renewable energy, inertia and damping, virtual synchronous generator (VSG), synchronous inertial reference coordinate (SIRC), HIL.**

I. INTRODUCTION

RENEWABLE energy is becoming more and more popular. This popularity and market share of renewable energy can be attributed to the fact that ever-increasing power electronics devices are penetrating into power systems to replace the conventional generation format. And this will address several common concerns related to the energy crisis and air pollution [1]-[3]. Fortunately, researchers have well acknowledged the importance of stability issues by continuously improving the stability analysis methods among the existing literature [4]-[20].

The authors Chang Li and Tomislav Dragicevic are with the Technical university of Denmark.

The author Yaqian Yang, Lei Wang are with the Hunan University of China.

The author Yijia Cao is with the Changsha university of Science and Technology

The author Frede Blaabjerg is with the Aalborg University.

Corresponding author: Chang Li, Yaqian Yang (Email: changlielektro@gmail.com, yaqianyang@hnu.edu.cn)

A virtual synchronous generator (VSG), which simulates the dynamic characteristics of a synchronous generator, can provide virtual inertia for the power system. Based on this virtual inertia concept, a hybrid energy storage system (ESS) and a novel VSG power management are proposed in [4] to achieve the reduction of the battery power fluctuations along with its changing rate. Beside of ESS applications, the VSG is widely applied to voltage source converters (VSCs). For example, in [5], VSG can be used in VSCs to realize self-synchronization by utilizing the dynamics of the DC-link capacitor. However, the active power oscillation may easily occur between two parallel synchronverters. Thus the suppression techniques are proposed in [6] during load fluctuations. Unfortunately, the weak power grid condition is not discussed in [6]. Another challenge is the lack of inertia, especially for small-scale modern power systems. To alleviate the inertia drop, the virtual inertia controls are recognized as the main solutions. However, as revealed in [7], the virtual inertia control may cause instabilities to the power converters under weak grid conditions. Thus, a modified virtual inertia control is proposed in [7] to improve the stability by mitigating the adverse effects. To improve the rate of change of frequency (RoCoF) and alleviate the frequency nadir, the power system inertia in [8] is emulated by energy stored in the dc-link capacitor of the converter through the proposed a virtual inertia control. Besides of frequency nadir and RoCoF caused by imbalanced active powers in the power system, another focused issue is oscillation-related stability, which originated from the interaction between the converter and weak grid.

Although VSG control can improve the transient response, i.e., frequency nadir and RoCoF [7]-[10], active power oscillation and improper transient active power-sharing can be observed when multiple inverters with VSG control are paralleled in microgrids [11]. Besides of operation of multiple paralleled VSGs, the integration of single VSG into the grid has a risk of instability as well, thus the parameter constraints are considered to guarantee the system more robust. As the same as the synchronous stability issue in inverter with a phase-locked loop (PLL) [12], the inverter with VSG control also exists synchronous stability issues [13]. However, besides of discussing the stability of VSG itself, it can help to enhance the stability margin and avoid instability of power electronic systems [14]-[16]. For example, a virtual synchronous

This article has been accepted for publication in a future issue of this journal, but has not been fully edited. Content may change prior to final publication. Citation information: DOI 10.1109/JESTPE.2020.3041698, IEEE Journal of Emerging and Selected Topics in Power Electronics

generator control strategy is proposed for damping DC resonance of the VSC-MTDC system, which fully exploits the potential inertia and damping ability of VSG control [14]. To strengthen the harmonics stability of the grid-tied inverter, a VSG control is applied to reshape the impedance of the converter to enhance the stability [15]. Furthermore, a VSG control with self-adaptive parameter tuning is proposed to dampen low frequency oscillation of power systems which is validated by IEEE 39-bus test system [16]. Besides of this, an impedance analysis is developed for the virtual synchronous generator to illustrate that virtual inertia can help to mitigate oscillation compared with conventional vector control [17]. Unfortunately, active power oscillation can occur when two VSGs are paralleled during load fluctuation, of which the mechanism was clarified by [6]. Besides enhancing the stability of AC grid by VSG control, the virtual inertia can also be employed to improve the stability as well as the damping performance of DC grid [18].

Besides of inverter with VSG control, the inverter with *dq* current control has a risk of small-signal instability as well, revealed by impedance analysis [19]. In regards to impedance modeling, the stability of grid-tied inverters has been discussed in [20], which shows that the negative incremental resistor can lead to grid synchronization instability. A phase-locked loop (PLL) is a critical element for the grid synchronization, especially in situations when the inverter controlled in *dq* synchronous reference frame. Thus low-frequency synchronous stability may occur if inappropriate control design is developed [21]. Angle stability, as a branch of stability problems, is a critical indicator of the capability of synchronization of the inverter with grid, which is discussed in [12].

Based on the above discussions, Comparison between different stability modeling methods and criteria are summarized in Table I. Besides, the distinction and contributions are highlighted by comparing different reference literatures with this paper, as shown in Table I, II, III, and IV, respectively.

TABLE I COMPARISON BETWEEN DIFFERENT REFERENCES

References	Contribution types
[4]-[5], [7]-[11]	Proposed new control approach
[6], [12]-[24]	Proposed new modeling method
[14], [16], [18], and this paper	Proposed new modeling method with stabilizing control

TABLE II CLASSIFICATION FOLLOWING DIFFERENT MODELING METHODS

References	Modeling methods
[12], [15], [17]-[23], and this paper	Impedance-based
[5]-[8], [11], [14], [16], [18]	Eigenvalue analysis
[6], [11], [13], [16]	State space representation
[5], [14], [18], and this paper	Closed-loop system

TABLE III CLASSIFICATION ACCORDING TO DIFFERENT CONTROL APPROACHES

References	Control approaches
[12], [19]-[23]	DQ-frame control with PLL
[4], [6], [13]-[15]	VSG control
[7]-[8], [18]	Virtual inertia control
[5], [9]-[11], [16]-[17], and this paper	Improved VSG control

TABLE IV CLASSIFICATION ACCORDING TO DIFFERENT TYPES OF STABILITY

References	Stability types
[5]-[6], [12]-[13]	Angle stability
[20]-[21], and this paper	Voltage stability
[7]-[11], [16], [20]-[21], and this paper	Frequency stability
[14], [18]	DC voltage stability

Besides of synchronous stability, subsynchronous oscillation belongs to another focused stability issue observed by the researchers [22]. As can be analogized with electromechanical oscillation of conventional synchronous generator, the wide frequency band oscillation may occur in the grid-tied VSG systems. To the best knowledge of the author, the voltage and frequency stability has not been discussed before. To fill in this blank, this paper focused on stability analysis of voltage and frequency of grid-tied VSG attached to a weak grid. Specifically, voltage stability analysis is developed by the proposed impedance modeling derived in the synchronous inertial reference coordinates (SIRC), where the rotational sinusoidal AC variables can be linearized around the operation point. Besides, frequency dynamics are analyzed by the proposed motion equation, where the stiffness was defined to illustrate the synchronizing capability of VSG with the weak grid. The main contributions of this paper are as follows:

1) An SIRC is proposed for the linearization of AC-side variables of the grid-tied VSG system, by which a new mathematical model is developed for voltage stability analysis.

2) The motion equation is proposed for the frequency stability of VSG. This proposed equation reveals that weaker grid strength means weaker grid stiffness, which brings weaker synchronization capability of VSG tracking with the grid.

3) Since the weaker grid stiffness may leads to the low-frequency oscillation, an inertia-damping-enhanced control method is proposed for VSG to improve frequency stability.

4) The theoretical analysis is demonstrated by the simulations and experiments.

The rest of this paper is organized as follows: Section II derives the mathematical model for frequency and voltage dynamic instability of grid-connected VSG. In Section III, impedance interaction analysis is provided for voltage oscillation. The proposed impedance model is well validated by the measured results. Also, frequency dynamics are identified by the motion equation. Besides, an inertia-damping-enhanced control method is proposed. In section IV, theoretical analysis is verified by experiments. Finally, section V draws the conclusions.

II. DYNAMIC MODEL OF VSG IN SIRC

In this section, the dynamic model of VSG is built in the synchronous inertial reference coordinate (SIRC) where the small-signal analysis can be developed. In this way, the impedance of both VSG and the weak grid was derived from developing voltage stability analysis. Before stability analysis, the definition of SIRC is firstly developed.

This article has been accepted for publication in a future issue of this journal, but has not been fully edited. Content may change prior to final publication. Citation information: DOI 10.1109/JESTPE.2020.3041698, IEEE Journal of Emerging and Selected Topics in Power Electronics

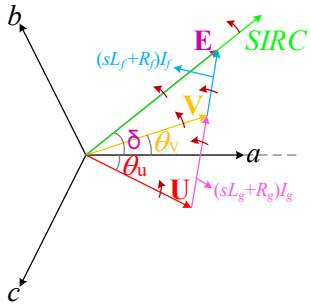

Fig. 1 Definition of SIRC

Fig. 1 presents the vectors of voltages and currents for a grid-tied VSG, of which all the quantities struggle to keep synchronized with SIRC. Different from the stationary natural coordinates, the defined SIRC rotates as a synchronous frequency. All the sinusoidal quantities can be transformed into DC components by reflecting in SIRC. As a result, voltage stability and frequency stability can be analyzed in the frame of SIRC.

A. Modeling of VSG in the SIRC

The three-phase power converter connected to the AC weak grid via an LC filter is shown in Fig. 2(a), where Z_{gn} is the grid impedance, R_{gn} is the parasitic resistance of the filter inductor, L_f and R_f represent filter inductance and the parasitic resistance, $\vec{\mathbf{V}}_\mathbf{f}$ is the three-phase voltage at the point of common coupling (PCC), $\vec{\mathbf{I}}_\mathbf{f}$ is the AC output current of the converter, $\vec{\mathbf{I}}_\mathbf{g}$ is the grid-integration current, $\vec{\mathbf{U}}_\mathbf{g}$ is the grid voltage, $\vec{\mathbf{E}}$ is the converter voltage. Fig. 2(b) shows the control scheme of the VSG. The active power controller of the VSG emulates the inertia and primary frequency regulation of synchronous machines, while the reactive power emulates the inertia and primary voltage regulation of the synchronous generator.

According to the topology of the grid-connected converter, the circuit voltage and current can be described as complex vectors as [23]:

$$\begin{cases} \vec{\mathbf{E}}(t)-\vec{\mathbf{V}}_\mathbf{f}(t)=Z_f\vec{\mathbf{I}}_\mathbf{f}(t) \\ \vec{\mathbf{I}}_\mathbf{f}(t)=\dfrac{1}{Z_c}\vec{\mathbf{V}}_\mathbf{f}(t)+\vec{\mathbf{I}}_\mathbf{g}(t) \\ \vec{\mathbf{V}}_\mathbf{f}(t)=\vec{\mathbf{U}}_\mathbf{g}(t)+Z_{fg}\vec{\mathbf{I}}_\mathbf{g}(t) \end{cases} \tag{1}$$

Furthermore, the time-domain circuit equations can be represented as, i.e.,

$$\begin{cases} Ee^{j\delta}-V_f e^{j\theta_V}=Z_f I_f e^{j\theta_{If}} \\ I_f e^{j\theta_{If}}=\dfrac{1}{Z_c}V_f e^{j\theta_V}+I_g e^{j\theta_{Ig}} \\ V_f e^{j\theta_V}=U_g e^{j\theta_U}+Z_{fg}I_g e^{j\theta_{Ig}} \end{cases} \tag{2}$$

where E, V_f, U_g, I_f, and I_g are the amplitudes of converter voltage, the PCC voltage, grid voltage, converter output current, and grid-integration current, δ, θ_V, θ_U, θ_{Ig}, and θ_{If} are the phase angles of converter voltage, PCC voltage, grid voltage, converter output current, and grid-integration current, respectively.

Since rotational variables are time-variant without static operating points, it is necessary to transform (2) into SIRC. Thus, all the variables can be linearized for small signal analysis. Thus, it yields:

$$\begin{cases} Ee^{j\delta}e^{-j\theta_U}-V_f e^{j\theta_V}e^{-j\theta_U}=Z_f I_f e^{j\theta_{If}}e^{-j\theta_U} \\ I_f e^{j\theta_{If}}e^{-j\theta_U}=\dfrac{1}{Z_c}V_f e^{j\theta_V}e^{-j\theta_U}+I_g e^{j\theta_{Ig}}e^{-j\theta_U} \\ V_f e^{j\theta_V}e^{-j\theta_U}=U_g e^{j\theta_U}e^{-j\theta_U}+Z_{fg}I_g e^{j\theta_{Ig}}e^{-j\theta_U} \end{cases} \tag{3}$$

As for grid-connected VSG, all the quantities contribute to tracking with the voltage of power grid and keep a synchronized rotation. Thus, all the phase angles can be recognized as the superposition of steady-state component and disturbed transient component, i.e.,

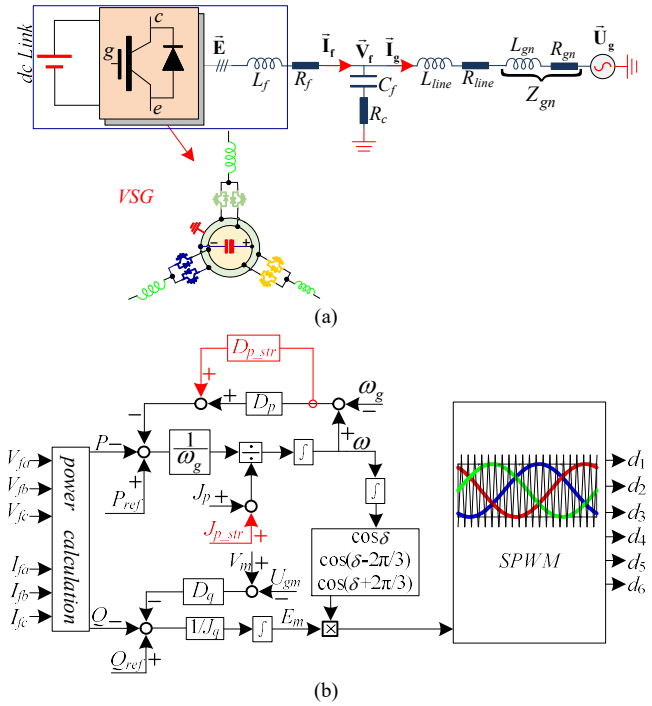

Fig. 2 Schematic of VSG attached to weak grid, (a) topology, (b) control strategy

$$\begin{cases} \delta=\omega t=(\omega_g+\mathrm{d}\omega)t=\theta_U+\mathrm{d}\delta \\ \theta_V=\omega_V t=(\omega_g+\mathrm{d}\omega_V)t=\theta_U+\mathrm{d}\theta_V \\ \theta_U=\omega_g t=(\omega_g+0)t=\theta_U+0 \end{cases} \tag{4}$$

where $\mathrm{d}\delta$ is the difference between the power angle of the AC output voltage of VSG and the power grid; and $\mathrm{d}\theta_V$ is the phase difference between the terminal voltage and the power grid. One can obtain that:

$$\begin{cases} \mathrm{d}\delta=\delta_0+\Delta\delta \\ \mathrm{d}\theta_V=\theta_{V0}+\Delta\theta_V \end{cases} \tag{5}$$

where δ_0 and θ_{V0} represent the equilibrium operation points of the difference of angles, $\Delta\delta$ and $\Delta\theta_V$ stand for small signal quantities of phase difference. With the coordinate transformation, AC voltage and current are time-invariant and can be linearized around operation points.

Substituting (4) into (3), one can obtain that

This article has been accepted for publication in a future issue of this journal, but has not been fully edited. Content may change prior to final publication. Citation information: DOI 10.1109/JESTPE.2020.3041698, IEEE Journal of Emerging and Selected Topics in Power Electronics

$$\begin{cases} Ee^{j\mathrm{d}\delta} - V_f e^{j\mathrm{d}\theta_V} = Z_f I_f e^{j\mathrm{d}\theta_{If}} \\ I_f e^{j\mathrm{d}\theta_{If}} = \dfrac{1}{Z_c} V_f e^{j\mathrm{d}\theta_V} + I_g e^{j\mathrm{d}\theta_{Ig}} \\ V_f e^{j\mathrm{d}\theta_V} = U_g e^{j0} + Z_{fg} I_g e^{j\mathrm{d}\theta_{Ig}} \end{cases} \tag{6}$$

where $\begin{cases} Z_f = R_f + sL_f \\ Z_c = R_c + \dfrac{1}{sC_f} \\ Z_{fg} = R_{line} + R_{gn} + s(L_{line} + L_{gn}) \end{cases}$

It should be noted that the small signal model of the phase difference with signs "d" is Δ after linearization.

Since VSG is to emulate the dynamic characteristics of SG, the active- and reactive controls of VSG can be expressed as:

$$\begin{cases} P_{ref} - P = J_p \omega_g \dfrac{d\omega}{dt} + D_p(\omega - \omega_g) \\ Q_{ref} - Q = J_q \dfrac{dE}{dt} + D_q(V_f - U_g) \end{cases} \tag{7}$$

where P is the feedback power; J_p and D_p stand for virtual inertia moment and virtual damping of active-power channel of VSG; J_q and D_q are virtual inertia moment and virtual damping of reactive-power channel of VSG.

According to Fig. 2, the output powers from VSG can be obtained as:

$$\begin{cases} P = \dfrac{EV_f}{|Z_f|}\cos(\varphi_{ff} - (\delta - \theta_V)) - \dfrac{V_f^2}{|Z_f|}\cos\varphi_{ff} \\ Q = \dfrac{EV_f}{|Z_f|}\sin(\varphi_{ff} - (\delta - \theta_V)) - \dfrac{V_f^2}{|Z_f|}\sin\varphi_{ff} \end{cases} \tag{8}$$

where E is the amplitude of output voltage of VSG; V_f is the amplitude of terminal voltage; φ_{ff} is the impedance angle of the impedance of $|Z_f|$, δ is output angle of VSG.

Combining (7) with (8), the small-signal model with linearization around steady working point is derived as:

$$\begin{cases} \Delta V_f = G_{VE}\Delta E + G_{V\delta}\Delta\delta \\ \Delta\theta_V = G_{\theta VE}\Delta E + G_{\theta V\delta}\Delta\delta \end{cases} \tag{9}$$

The original definition of complex power can be obtained as:

$$\begin{aligned} &\tilde{S} = \mathbf{V}\mathbf{I}^* \\ &\Rightarrow V_f e^{j\theta_V} I_f e^{-j\theta_{If}} \Rightarrow V_f I_f e^{j\phi} \\ &\Rightarrow \begin{cases} P = V_f I_f \cos\phi \\ Q = V_f I_f \sin\phi \end{cases} \end{aligned} \tag{10}$$

where ϕ is the power factor angle, which is the phase difference between θ_V and θ_{If}. The above (10) can be linearized as:

$$\begin{cases} \Delta\tilde{S} = (V_{f0}\Delta I_f + I_{f0}\Delta V_f)e^{j\phi_0} + je^{j\phi_0} S_0(\Delta\theta_V - \Delta\theta_{If}) \\ \Delta Q = (V_{f0}\Delta I_f + I_{f0}\Delta V_f)\sin\phi_0 + S_0\cos\phi_0(\Delta\theta_V - \Delta\theta_{If}) \end{cases} \tag{11}$$

where ϕ_0 is the steady point of power factor angle, S_0 is the steady operation point of complex power, i.e., $S_0 = V_{f0}I_{f0}$; It can be inferred that the SIRC cannot change the apparent power, active power and reactive power as another advantage of the proposed SIRC.

The apparent power S_1 is expressed as:

$$\begin{aligned} &S = \sqrt{P^2 + Q^2} \\ &\Rightarrow \Delta S = \frac{P_0\Delta P + Q_0\Delta Q}{S_0} \end{aligned} \tag{12}$$

Combining (8) with (12), the small-signal model can be derived as:

$$\begin{cases} \Delta S = B_1(\Delta\delta - \Delta\theta_V) + B_2\Delta V_f + B_3\Delta E \\ \Delta Q = A_1(\Delta\delta - \Delta\theta_V) + A_2\Delta E + A_3\Delta V_f \end{cases} \tag{13}$$

where the detailed representations of A_1, A_2, A_3, B_1, B_2, and B_3 can be seen in the Appendix.

Combining (6), (9), with (12), one can derive that:

$$\Delta\theta_{If} = C_1\Delta\delta + C_2\Delta\theta_V + C_3\Delta E + C_4\Delta V_f \tag{14}$$

Substituting (7) into (14) and combining (11)-(13), the equivalent impedance of VSG is obtained as:

$$Z_{vsg} = -\frac{\mathbf{\Delta V_f}}{\mathbf{\Delta I_f}} = -\frac{e^{j\theta_{V0}}K_1 + je^{j\theta_{V0}}V_{f0}K_2}{e^{j\theta_{If0}}K_3 + je^{j\theta_{If0}}I_{f0}K_4} \tag{15}$$

where $\begin{cases} K_1 = G_{VE}G_{E\delta} + G_{V\delta} \\ K_2 = G_{\theta VE}G_{E\delta} + G_{\theta V\delta} \\ K_3 = H_3 + H_4G_{E\delta} \\ K_4 = H_1 + H_2G_{E\delta} \end{cases}$

As a result, the output impedance of VSG can be re-written as:

$$Z_{vsg} = -\frac{\mathbf{\Delta V_f}}{\mathbf{\Delta I_f}} = -\frac{e^{j\theta_{V0}}K_1 + je^{j\theta_{V0}}V_{f0}K_2}{e^{j\theta_{If0}}K_3 + je^{j\theta_{If0}}I_{f0}K_4} \tag{16}$$

The grid impedance is derived as:

$$Z_{grid} = \frac{\mathbf{\Delta V_f}}{\mathbf{\Delta I_g}} // Z_c(s + j\omega_0) \tag{17}$$

The derived impedance is the closed-loop equivalent impedance, which contains both circuit parts and control parts. The dark $\mathbf{\Delta V_f}$ and $\mathbf{\Delta I_f}$ represent the DC components of voltage and current, which are transformed into rotational coordinates.

III. Stability Analysis of Voltage and Frequency

Based on the derived impedance model, both voltage and frequency stability analysis are developed in this section.

A. Voltage stability analysis

Fig. 3 shows the impedances of Z_{vsg} and Z_{grid} with various grid strengths. The yellow points are the measured results of VSG impedances. Both the electrical components and control parts of a closed-loop system are built in the environment of SIMULINK. Then, an extra input perturbation is imposed on the circuit, and the output measurement is equipped to get the expected terminal characteristics. It can be noted that the excitation source with 50 Hz has no need to be stimulated here due to the weak response. Then, by means of SIRC transformation, the frequency response can be estimated at the selected frequency ranges. Measured results match with that of the derived impedance, validating effectiveness of the proposed impedance modeling.

This article has been accepted for publication in a future issue of this journal, but has not been fully edited. Content may change prior to final publication. Citation information: DOI 10.1109/JESTPE.2020.3041698, IEEE Journal of Emerging and Selected Topics in Power Electronics

As shown in Fig. 3(a), the VSG impedance intersected with grid impedance within 20 to 30 rad/s, where $|Z_{vsg}|>|Z_{grid}|$, and the phase difference is around -245 degrees. It indicates that the Nyquist curve of the minor loop gain (impedance ratio) has two crossings beyond the point (-1, j0). Meanwhile, in Fig. 4(a), the amount of right half-plane pole (RHPP) is 1, which can be inferred that the system is unstable because the amounts of crossings are not as large as the RHPP amounts [24]. An intersection point exists within higher-frequency regions, at which the phases of Z_{vsg} and Z_{grid} are 90 degrees and -90 degrees, respectively, suggesting the dynamic interactive behavior with poor damping.

Fig. 3(b) and Fig. 4(b) indicates that the cascaded system of Z_{vsg}/Z_{grid} is unstable where the phase difference is around -200 degrees at the intersection point between VSG impedance and grid impedance, meanwhile, only one RHPP occurs.

It can be inferred that low-frequency and high-frequency instability has a risk of occurring simultaneously because of the undesired impedance interaction between VSG and weak grid.

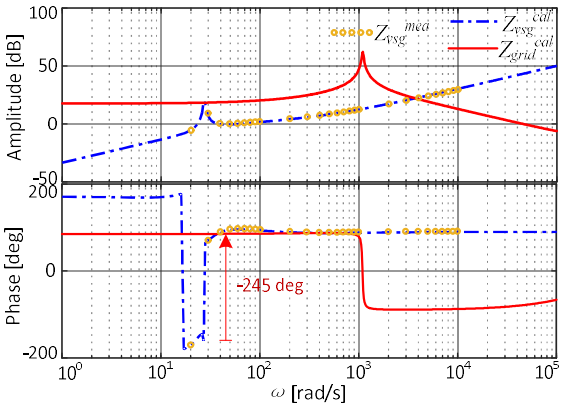

Fig. 3 Impedance frequency characteristics of grid-tied VSG and power grid, (a) short circuit ratio (SCR)=2, (b) SCR=1

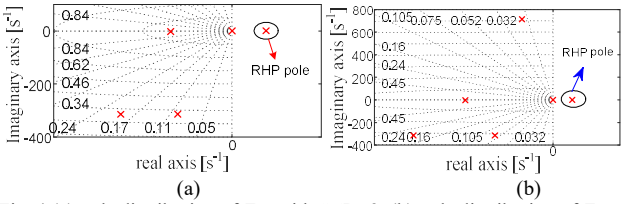

Fig. 4 (a) pole distribution of Z_{vsg} with SCR=2, (b) pole distribution of Z_{vsg} with SCR=1.

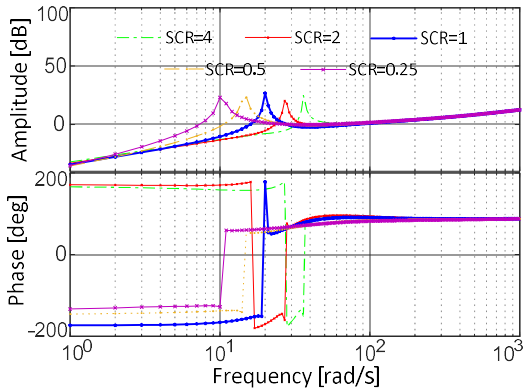

Fig. 5 VSG impedance with various short circuit ratio

Fig. 5 shows the frequency response characteristics of VSG impedance, where it can be seen that no matter of weaker grid stiffness or stronger grid stiffness, the impedance has a resonance peak within the lower-frequency bands. Furthermore, the resonance frequency moves to the lower frequency bands as the grid stiffness gets weaker, indicating that the risk of low-frequency oscillation existed. Besides, VSG impedance behaves characteristics of non-passivity within lower-frequency bands, suggesting a high risk of instability [25].

B. Frequency dynamics analysis of VSG

The above discussion is mainly focused on the impedance interaction between VSG and weak grid, for AC voltage amplitude oscillation analysis. As shown in Fig. 5, the resonance peaks appear when grid stiffness is low. The peaks can lead to voltage oscillation and thus result in frequency oscillation. This part concentrated on the frequency dynamics of VSG with the amplitude-phase motion equation [26].

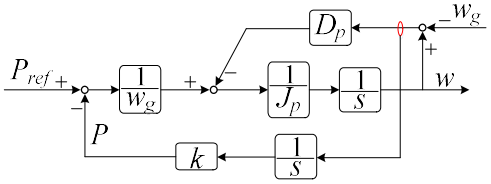

Fig. 6 Swing equation of active power-frequency channel of VSG

As shown in Fig. 6, it can be inferred that the frequency dynamics contribute to negative feedback to stabilize active power through two channels when the system is subjected to a power disturbance. To be specific, if the input power is increased, the output frequency of VSG is naturally increased until the real P has reached to P_{ref} by the damping power. However, the synchronous- and damping-power meanwhile increase because of positive D_p and k, as the frequency is increased. In this manner, the angular frequency of VSG would not be continuously ascended until the net input active power is equal to zero.

Like this, the dynamic response of frequency will periodically change along with this law. Therefore, the net power is the original cause of the motion of angular frequency of VSG, but larger virtual inertia can always better hinder the motion of angular frequency not only for lower RoCoF but also for frequency nadir.

Further, based on Fig. 6, the dynamic differential equation

This article has been accepted for publication in a future issue of this journal, but has not been fully edited. Content may change prior to final publication. Citation information: DOI 10.1109/JESTPE.2020.3041698, IEEE Journal of Emerging and Selected Topics in Power Electronics

can be acquired as:

$$\begin{cases} P_{ref}\text{-}P = J_p\omega_g \dfrac{d\omega}{dt} + D_p(\omega\text{-}\omega_g) \\ J_p\omega_g \dfrac{d^2\omega}{dt^2} + D_p \dfrac{d\omega}{dt} + k(\omega\text{-}\omega_g) = 0 \end{cases} \tag{18}$$

It can be concluded from (18) that larger J_p can lead to slower RoCoF and a lower rate of change of acceleration (RoCoA) (acceleration is defined as $d^2\omega/dt^2$). The larger D_p can not only result in lower RoCoF, but also lead to less dynamic frequency deviation in the transients.

The sign k is defined as the "synchronization coefficient" or "stiffness coefficient" because k contributes to making ω track well with ω_g in the transients. In another view, k is inversely proportional to the amplitude of system impedance ($\sqrt{(R_{line}+R_{gn})^2+(\omega(L_{line}+L_{gn}))^2}$). It is indicated that larger system impedance leads to a smaller stiffness coefficient, i.e., weaker grid strength. Hence, it is concluded that k is the stiffness- or synchronizing-coefficient, which is to help VSG track with the grid. Hence, a larger synchronization coefficient results in a stronger synchronized capability of VSG tracking with a weak power grid.

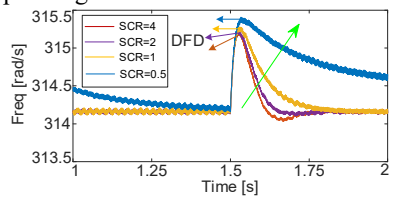

Fig. 7 The impact of various sizes of stiffness coefficient on frequency dynamics

In Fig. 7, DFD means the dynamic frequency deviations, it can be inferred that stronger stiffness, i.e., the closer electrical connection between VSG and grid, can lead to smaller DFD. Especially for the ultra-weak power grid, DFD is evidently increased, which seriously impede the frequency returning back to the nominal value. In general, strong enough grid strength is good for frequency robustness.

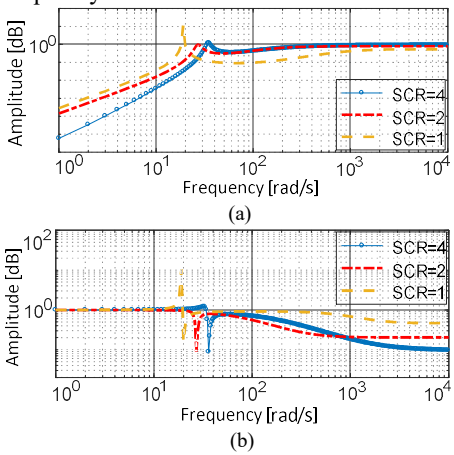

Fig. 8 Robustness analysis of VSG frequency, (a) Sensitivity function, (b) Complementary sensitivity function

To illustrate the impact of grid stiffness on VSG frequency dynamics, both sensitivity and complementary sensitivity are obtained to develop robustness analysis and robust stability analysis [27]. Nominal performance is generally evaluated by sensitivity S, and robust stability is identified by complementary sensitivity T, moreover, the robustness performance is judged by the infinite form of sum of S and T, i.e.,

$$\begin{cases} NP \Leftrightarrow |S|_\infty \le 1 \\ RS \Leftrightarrow |T|_\infty \le 1 \\ RP \Leftrightarrow \max_\omega(|S|_\infty + |T|_\infty) \le 1 \end{cases} \tag{19}$$

where

$$\begin{cases} S = \dfrac{1}{1+L} \\ T = \dfrac{L}{1+L} \end{cases}$$

where L represents the open-loop gain of the closed-loop control system, $|S|_\infty$ means the infinite-norm of sensitivity, and $|T|_\infty$ means the infinite-norm of complementary sensitivity. Besides, the signs *NP*, *RS*, and *RP* represent nominal performance, robust stability, and robustness performance, respectively.

It can be seen in Fig. 8(a), the infinite-norm of $|S|_\infty$ is nearly as large as 1 with SCR=4 and SCR=2, but $|S|_\infty > 1$ with SCR=1. Therefore, the weaker grid strength aggravates the nominal performance of the system, and the frequency of VSG has a high risk of low-frequency oscillation. Besides, the complementary sensitivity has a similar resonance peak compared with sensitivity, which indicates the frequency has a risk of appearing low-frequency oscillation. Thus, the robust stability and robustness performance are deteriorated by the weak grid strength and low grid stiffness.

Because of $|S|_\infty > 1$ and $|T|_\infty > 1$, it is hard to guarantee good robust stability and robustness as for frequency. It illustrates that the weaker stiffness and weaker grid strength suggest poorer frequency robustness as well as robust stability.

C. The strengthened virtual inertia and virtual damping control for suppressing frequency oscillation

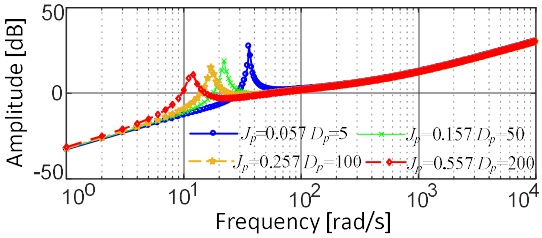

Fig. 9 The impact of virtual inertia and virtual damping on VSG impedance characteristics

Fig. 9 illustrates the VSG impedance characteristics under various virtual inertia and virtual damping. Fig. 9 shows that the larger virtual inertia and virtual damping constants mean the lower resonance peaks. It indicates the larger virtual inertia and virtual damping can enlarge the damping performance of VSG impedance and improve stability margins.

Based on this idea, strengthened virtual inertia and virtual damping control are proposed to improve the frequency stability and dampen frequency oscillation.

This article has been accepted for publication in a future issue of this journal, but has not been fully edited. Content may change prior to final publication. Citation information: DOI 10.1109/JESTPE.2020.3041698, IEEE Journal of Emerging and Selected Topics in Power Electronics

The strengthened virtual inertia and virtual damping control links are added with the red signs, as shown in Fig. 2(b). It should be noted that the control parameters design generally has not taken the interaction between VSG and the grid. Hence, it is reasonable to add the supplementary control for mitigating the frequency oscillation.

To further validate the proposed control method, the robustness and robust stability are evaluated for frequency with the help of sensitivity- and complementary sensitivity functions.

As shown in Fig. 10, both complementary sensitivity and sensitivity functions are obtained to judge the robust stability and robustness of the system.

It can be seen that there appear peaks in both T and S, and the value of $|S|_\infty$ and $|T|_\infty$ is much larger than 1, which indicates that stability and robustness of the frequency cannot be guaranteed. However, the peaks decline a lot with adopting the strengthened control method. The peaks of complementary sensitivity T gets lower as J_{p_str} becomes larger. Although the same law is not applicable for the change of sensitivity function S, the peaks are lessened much, the value of which are below 1.

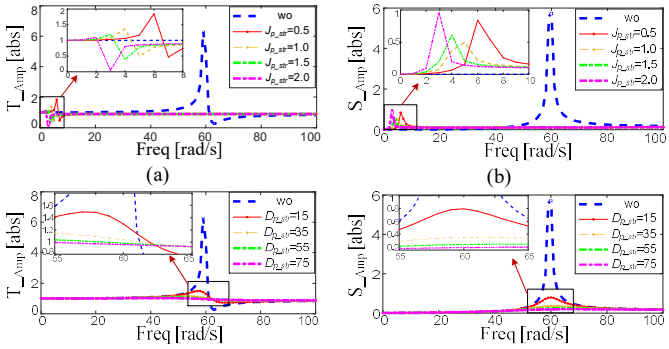

Fig. 10 Identification of robustness and robust stability, (a) complementary sensitivity with various J_{p_str}, (b) sensitivity with various J_{p_str}, (c) complementary sensitivity with various D_{p_str}, (d) sensitivity with various D_{p_str}

Fig. 10(c) and (d) display S and T as the control parameters D_{p_str} gets changed. When no supplementary control schemes are introduced, the robustness and robust stability is poor due to the high infinite norm of sensitivity and complementary sensitivity. However, the strengthened control strategy helps to lessen the peaks to a safe region to guarantee the good robustness and robust stability. Besides, the peak gets lower when D_{p_str} gets larger. It can be seen that the proposed control strategy can guarantee the robustness and robust stability of VSG even in the weak AC grid conditions.

D. Simulations verifications

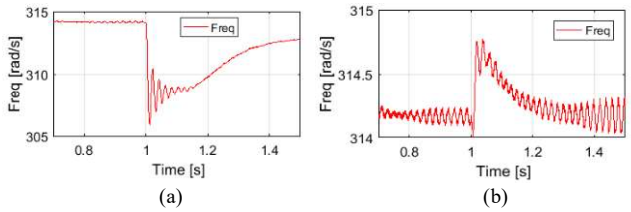

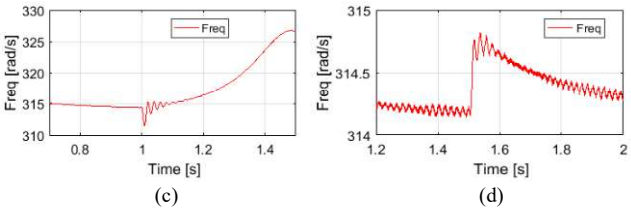

Fig. 11 The frequency dynamics of VSG attached to weak AC power grid, (a) SCR=2 with Δf=-0.2 Hz, (b) SCR=2 dropping with 10% nominal voltage, (c) SCR=1 with Δf=-0.2 Hz, (d) SCR=1 dropping with 10% nominal voltage

As can be seen in Fig. 11(b) and (d), active power oscillated with slip angular frequency over time because the VSG frequency cannot track well with grid frequency. Then it is coupled with frequency via active-channel of VSG control within the bandwidth. Thus, the frequency oscillation has been stimulated.

Compared Fig. 11(b) with Fig. 11(d), VSG frequency can successfully return to the initial value by tracking well with grid frequency when SCR=2. However, it is hard to return to the nominal value to maintain synchronization after disturbance, when SCR=1. Thus, weaker grid stiffness would result in poorer synchronization ability. It indicates that VSG tracks with the grid more difficult.

Compared Fig. 11(a) with Fig. 11(c), it can be inferred that the lower SCR can make VSG not track well with the grid and lose synchronization after disturbance. However, the higher SCR can make the frequency restore to the nominal value after a disturbance. It can be inferred that higher SCR means the stronger synchronized capability of VSG tracking with the grid.

Fig. 12 shows the simulations of active- and reactive power in the same scenarios, as that in Fig. 11. In Fig. 12(a), both active- and reactive-power is sharply increased to compensate for the power shortage to make the frequency restoring. Until the frequency reaches the steady-state, the powers gradually tend to be stable. In Fig. 12(c), the active- and reactive-power deviate from the given value, which corresponds to the dynamics of frequency.

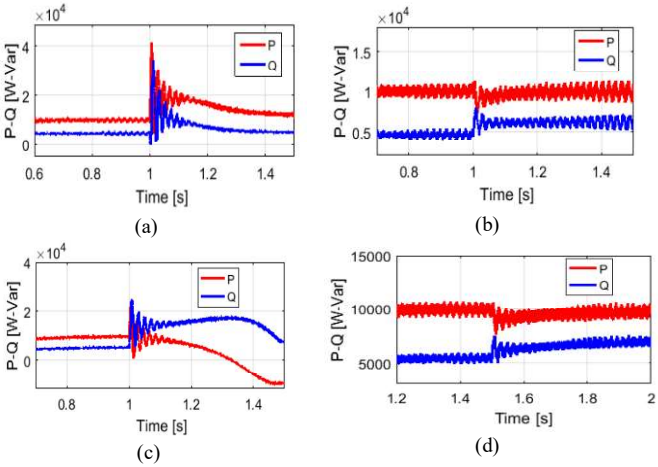

Fig. 12 The power dynamics of VSG, (a) SCR=2 with Δf=-0.2 Hz, (b) SCR=2 dropping with 10% nominal voltage, (c) SCR=1 with Δf=-0.2 Hz, (d) SCR=1 dropping with 10% nominal voltage

Fig. 13 illustrates the relationship between SCR and synchronizing ability. The synchronizing ability is measured by the defined grid stiffness. Synchronizing ability is poor when SCR is low, and the synchronizing capability is strengthened as

This article has been accepted for publication in a future issue of this journal, but has not been fully edited. Content may change prior to final publication. Citation information: DOI 10.1109/JESTPE.2020.3041698, IEEE Journal of Emerging and Selected Topics in Power Electronics

SCR gets larger. It can be inferred that the ultra-weak grid is not suitable for the integration of VSG and will lead to the potential frequency stability issue.

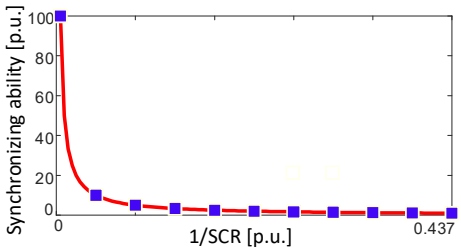

Fig. 13 The relationship between SCR and synchronizing ability of VSG

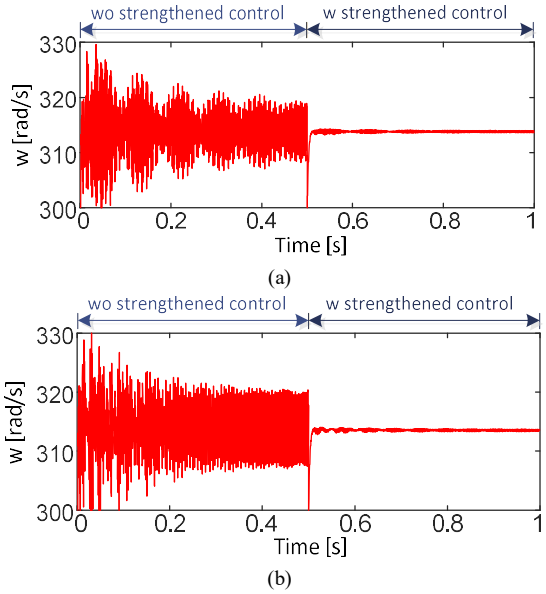

Fig. 14 Inertia-strengthened stabilizing control to dampen frequency oscillation (SCR=1, D_p=50, J_q=0.71, D_q=321), (a) J_p=0.0057, (b) J_p=0.017

Fig. 14 shows the frequency instability when VSG is attached to a weak grid with inappropriate control settings. With the given control parameters settings, frequency is prone to high-frequency oscillation due to the dynamic interactions between VSG and weak grid. However, the oscillation can be well suppressed with the proposed inertia-strengthened control method, well validating the effectiveness of the proposed inertia-strengthened control.

IV. Validations

To demonstrate the theoretical analysis, the experimental results based on control hardware in the loop are carried out in this section. The system parameters are shown in Table V, and the control parameters of VSG can be referring to [28], [29].

TABLE V System Parameters

Converter-side filter inductance	3.2 mH
Parasitic resistance R_f	0.1 Ω
Filter capacitance	22 μF
Parasitic resistance R_c	0.2 Ω
Grid-side filter inductance	3 mH
Parasitic resistance R_g	0.4 Ω
Virtual inertia (active) J_p	0.057
Virtual damping (active) D_p	5
Virtual inertia (reactive) J_q	7.1
Virtual damping (reactive) D_q	321
Rated power	23 kW
Nominal grid line voltage	380 V
DC voltage	800 V
Switching frequency	10 kHz

Fig. 15 shows the three-phase voltages with various SCRs, which can be seen that the voltages are distorted due to the low SCR as well as weak grid stiffness. It can be inferred that AC voltages are more prone to distortion or instability when VSG is attached to the weak-stiffness grid.

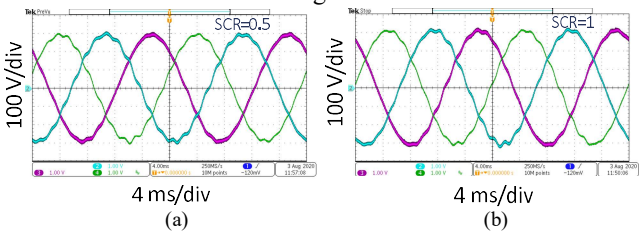

Fig. 15 Three-phase voltage with various grid stiffness, (a) SCR=1, (b) SCR=0.5

Fig. 16(a) and (c) present the dynamic response of frequency, active- and reactive-power during start-up with various grid SCRs. It can be seen that active- and reactive-power oscillation appears in both cases. The real active- and reactive power can track well with the given value (P_{ref}=10 kW, Q_{ref}=0 var) when SCR=2. However, the reactive power cannot track with the reference when SCR=0.5. It can be seen that the weaker grid stiffness can impose a negative effect on the steady-state performance of the reactive power. Besides, both active- and reactive-power are oscillated with a small fluctuation range.

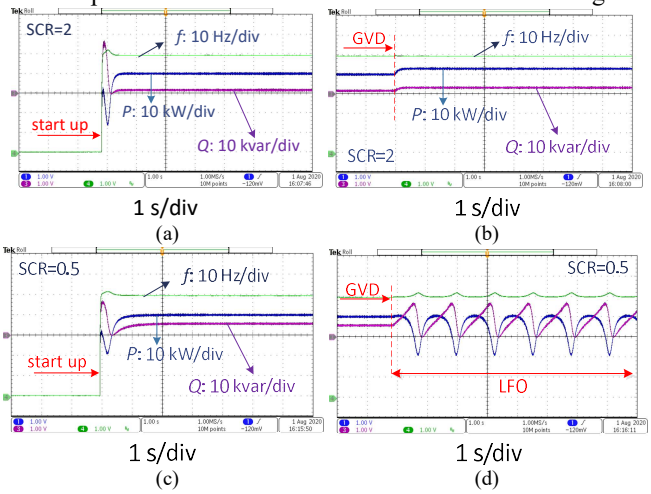

Fig. 16 The dynamics of active power, reactive power, and frequency, (a) SCR=2 during start-up, (b) SCR=2 with disturbance of grid voltage (GVD), (c) SCR=0.5 during start-up, (d) SCR=0.5 with GVD

A disturbance with 10% voltage drops is developed for SCR=2 and SCR=0.5, respectively, which can be shown in Fig. 16(b) and (d). The system can still maintain stable operation with varying operation points when SCR=2. However, frequency, active- and reactive-power appear to be low-frequency oscillation (LFO) when SCR=0.5. It illustrates the weaker grid strength is more unfavorable stable operation of the system and can lead to frequency and power oscillation during GVD.

Fig. 17 shows the dynamic responses with grid frequency disturbance (GFD). It can be observed that system can maintain stable operation when SCR=2. However, the LFO appears when SCR=0.5, which well illustrates frequency stability becomes worse when grid stiffness gets weaker.

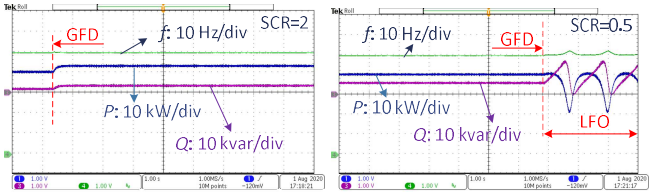

Fig. 17 The dynamics of active power, reactive power, and frequency with GFD, (a) SCR=2, (b) SCR=0.5

V. Conclusions

A new mathematical model has been proposed for voltage and frequency stability analysis of grid-tied VSG attached to a weak grid. The proposed model facilitated the voltage- and frequency-stability analysis. The impedance analysis has shown that VSG interacted with the weak grid and thus excited the low- and high-frequency oscillation. Meanwhile, the frequency robustness has been discussed with considering various grids stiffness. Besides, the capability of synchronization was studied with a VSG. Moreover, the relationship between the grid stiffness and synchronizing ability has been discussed. It was found that stronger stiffness is better for VSG to keep synchronized with the grid during disturbance.

Besides, an inertia-damping-enhanced method has been proposed for improving frequency dynamics response and enlarging stability margin. Finally, the proposed conceives have been demonstrated by the simulations and experiments.

VI. Discussions

Today, virtual synchronous generator (VSG) techniques have been a very popular one in the low-inertia power systems as it can help to enhance the inertia and damping for the systems with integration of large amounts of renewable energy. However, alike the conventional SG, the wideband oscillation are frequently occurring in the VSG-based power systems, which is urgently to be tackled.

The main works of this paper are organized as follows:

1) The small signal model is built in the proposed SIRC, which can be used to identify the voltage stability. SIRC is convenient to be implemented.

2) The frequency stability is developed by the proposed motion equation. And the synchronism as well as oscillation of frequency can be judged by the built motion equation.

3) To mitigate the oscillation of frequency, an inertia-damping-enhanced control method is proposed to improve frequency stability.

4) It provides a new perspective for the future study of voltage, frequency, even angle stability of power systems with high penetration of renewable energy considering other control schemes and topologies.

References

[1] J. Yuan, F. Blaabjerg, Y. Yang, A. Sangwongwanich and Y. Shen, "An Overview of Photovoltaic Microinverters: Topology, Efficiency, and Reliability," *2019 IEEE 13th International Conference on Compatibility, Power Electronics and Power Engineering (CPE-POWERENG)*, Sonderborg, Denmark, 2019, pp. 1-6.

[2] J. Yuan, F. Blaabjerg, Y. Yang, A. Sangwongwanich and Y. Shen, "An Overview of Photovoltaic M icroinverters: Topology, Efficiency, and Reliability," *2019 IEEE 13th International Conference on Compatibility, Power Electronics and Power Engineering (CPE-POWERENG)*, Sonderborg, Denmark, 2019, pp. 1-6.

[3] Z. Chen, J. M. Guerrero and F. Blaabjerg, "A Review of the State of the Art of Power Electronics for Wind Turbines," in IEEE Transactions on Power Electronics, vol. 24, no. 8, pp. 1859-1875, Aug. 2009.

[4] J. Fang, Y. Tang, H. Li and X. Li, "A Battery/Ultracapacitor Hybrid Energy Storage System for Implementing the Power Management of Virtual Synchronous Generators," in IEEE Transactions on Power Electronics, vol. 33, no. 4, pp. 2820-2824, April 2018.

[5] L. Huang et al., "A Virtual Synchronous Control for Voltage-Source Converters Utilizing Dynamics of DC-Link Capacitor to Realize Self-Synchronization," in IEEE Journal of Emerging and Selected Topics in Power Electronics, vol. 5, no. 4, pp. 1565-1577, Dec. 2017.

[6] Z. Shuai, W. Huang, Z. J. Shen, A. Luo and Z. Tian, "Active Power Oscillation and Suppression Techniques Between Two Parallel Synchronverters During Load Fluctuations," in IEEE Transactions on Power Electronics, vol. 35, no. 4, pp. 4127-4142, April 2020.

[7] J. Fang, P. Lin, H. Li, Y. Yang and Y. Tang, "An Improved Virtual Inertia Control for Three-Phase Voltage Source Converters Connected to a Weak Grid," in IEEE Transactions on Power Electronics, vol. 34, no. 9, pp. 8660-8670, Sept. 2019.

[8] J. Fang, H. Li, Y. Tang and F. Blaabjerg, "Distributed Power System Virtual Inertia Implemented by Grid-Connected Power Converters," in IEEE Transactions on Power Electronics, vol. 33, no. 10, pp. 8488-8499, Oct. 2018.

[9] D. Li, Q. Zhu, S. Lin and X. Y. Bian, "A Self-Adaptive Inertia and Damping Combination Control of VSG to Support Frequency Stability," in IEEE Transactions on Energy Conversion, vol. 32, no. 1, pp. 397-398, March 2017.

[10] J. Alipoor, Y. Miura and T. Ise, "Power System Stabilization Using Virtual Synchronous Generator With Alternating Moment of Inertia," in IEEE Journal of Emerging and Selected Topics in Power Electronics, vol. 3, no. 2, pp. 451-458, June 2015.

[11] J. Liu, Y. Miura, H. Bevrani and T. Ise, "Enhanced Virtual Synchronous Generator Control for Parallel Inverters in Microgrids," in IEEE Transactions on Smart Grid, vol. 8, no. 5, pp. 2268-2277, Sept. 2017.

[12] H. Lin, C. Jia, J. M. Guerrero and J. C. Vasquez, "Angle Stability Analysis for Voltage-Controlled Converters," in IEEE Transactions on Industrial Electronics, vol. 64, no. 8, pp. 6265-6275, Aug. 2017.

[13] W. Du, Q. Fu and H. F. Wang, "Power System Small-Signal Angular Stability Affected by Virtual Synchronous Generators," in IEEE Transactions on Power Systems, vol. 34, no. 4, pp. 3209-3219, July 2019.

[14] C. Li, Y. Li, Y. Cao, H. Zhu, C. Rehtanz and U. Häger, "Virtual Synchronous Generator Control for Damping DC-Side Resonance of VSC-MTDC System," in IEEE Journal of Emerging and Selected Topics in Power Electronics, vol. 6, no. 3, pp. 1054-1064, Sept. 2018.

[15] W. Wu et al., "Sequence Impedance Modeling and Stability Comparative Analysis of Voltage-Controlled VSGs and Current-Controlled VSGs," in IEEE Transactions on Industrial Electronics, vol. 66, no. 8, pp. 6460-6472, Aug. 2019.

[16] W. Wang, L. Jiang, Y. Cao and Y. Li, "A Parameter Alternating VSG Controller of VSC-MTDC Systems for Low Frequency Oscillation Damping," in IEEE Transactions on Power Systems. doi: 10.1109/TPWRS.2020.2997859

[17] A. Asrari, M. Mustafa, M. Ansari and J. Khazaei, "Impedance Analysis of Virtual Synchronous Generator-Based Vector Controlled Converters for Weak AC Grid Integration," in IEEE Transactions on Sustainable Energy, vol. 10, no. 3, pp. 1481-1490, July 2019.

[18] Y. Yang, C. Li, J. Xu, F. Blaabjerg and T. Dragicevic, "Virtual Inertia Control Strategy for Improving Damping Performance of DC Microgrid with Negative Feedback Effect," in IEEE Journal of Emerging and Selected Topics in Power Electronics.

[19] B. Wen, R. Burgos, D. Boroyevich, P. Mattavelli and Z. Shen, "AC Stability Analysis and dq Frame Impedance Specifications in Power-Electronics-Based Distributed Power Systems," in IEEE Journal of Emerging and Selected Topics in Power Electronics, vol. 5, no. 4, pp. 1455-1465, Dec. 2017.

[20] B. Wen, D. Boroyevich, R. Burgos, P. Mattavelli and Z. Shen, "Analysis of D-Q Small-Signal Impedance of Grid-Tied Inverters," in IEEE Transactions on Power Electronics, vol. 31, no. 1, pp. 675-687, Jan. 2016.

[21] D. Dong, B. Wen, D. Boroyevich, P. Mattavelli and Y. Xue, "Analysis of Phase-Locked Loop Low-Frequency Stability in Three-Phase Grid-Connected Power Converters Considering Impedance Interactions," in IEEE Transactions on Industrial Electronics, vol. 62, no. 1, pp. 310-321, Jan. 2015.

[22] K. Sun, W. Yao, J. Fang, X. Ai, J. Wen and S. Cheng, "Impedance Modeling and Stability Analysis of Grid-Connected DFIG-Based Wind Farm With a VSC-HVDC," in IEEE Journal of Emerging and Selected Topics in Power Electronics, vol. 8, no. 2, pp. 1375-1390, June 2020.

[23] L. Harnefors, M. Bongiorno, and S. Lundberg, "Input-admittance calculation and shaping for controlled voltage-source converters," IEEE Trans. Ind. Electron., vol. 54, no. 6, pp. 3323–3334, Dec. 2007.

[24] Y. Liao and X. Wang, "Impedance-Based Stability Analysis for Interconnected Converter Systems With Open-Loop RHP Poles," in *IEEE Transactions on Power Electronics*, vol. 35, no. 4, pp. 4388-4397, April 2020.

[25] L. Harnefors, X. Wang, A. G. Yepes and F. Blaabjerg, "Passivity-Based Stability Assessment of Grid-Connected VSCs—An Overview," in IEEE Journal of Emerging and Selected Topics in Power Electronics, vol. 4, no. 1, pp. 116-125, March 2016.

[26] P. Kundur, Power System Stability and Control. New York, NY, USA: McGraw-Hill, 1994.

[27] S. Skogestad and I. Postlethwaite, Multivariable Feedback Control: Analysis and Design, 2nded. Hoboken,NJ,USA:Wiley,2005.

[28] H. Wu *et al*., "Small-Signal Modeling and Parameters Design for Virtual Synchronous Generators," in *IEEE Transactions on Industrial Electronics*, vol. 63, no. 7, pp. 4292-4303, July 2016.

[29] Z. Song *et al*., "Small signal modeling and parameter design of virtual synchronous generator to weak grid," *2018 13th IEEE Conference on Industrial Electronics and Applications (ICIEA)*, Wuhan, 2018, pp. 2618-2624.